nature Accelerated Article Preview

LETTER
doi:10.1038/nature26156

Modular assembly of the nucleolar pre-60S ribosomal subunit

Zahra Assur Sanghai, Linamarie Miller, Kelly R. Molloy, Jonas Barandun, Mirjam Hunziker, Malik Chaker-Margot, Junjie Wang, Brian T. Chait and Sebastian Klinge

Cite this article as: Sanghai, Z. A. *et al.* Modular assembly of the nucleolar pre-60S ribosomal subunit. *Nature* http://dx.doi.org/10.1038/nature26156 (2018).

Received 30 November 2017; accepted 23 February 2018.
Accelerated Article Preview Published online 5 March 2018.

LETTER

doi:10.1038/nature26156

Modular assembly of the nucleolar pre-60S ribosomal subunit

Zahra Assur Sanghai[1,2], Linamarie Miller[1,2,3], Kelly R. Molloy[4], Jonas Barandun[2], Mirjam Hunziker[2], Malik Chaker-Margot[2,3], Junjie Wang[4], Brian T. Chait[4] and Sebastian Klinge[2]

Early co-transcriptional events of eukaryotic ribosome assembly result in the formation of precursors of the small (40S) and large (60S) ribosomal subunits[1]. A multitude of transient assembly factors regulate and chaperone the systematic folding of pre-ribosomal RNA subdomains. However, due to limited structural information, the role of these factors during early nucleolar 60S assembly is not fully understood. Here we have determined cryo-EM reconstructions of the nucleolar pre-60S ribosomal subunit in different conformational states at resolutions up to 3.4 Å. These reconstructions reveal how steric hindrance and molecular mimicry are used to prevent both premature folding states and binding of later factors. This is accomplished by the concerted activity of 21 ribosome assembly factors that stabilize and remodel pre-ribosomal RNA and ribosomal proteins. Among these factors, three Brix-domain proteins and their binding partners form a ring-like structure at rRNA domain boundaries to support the architecture of the maturing particle. Mutually exclusive conformations of these pre-60S particles suggest that the formation of the polypeptide exit tunnel is achieved through different folding pathways during subsequent stages of ribosome assembly. These structures rationalize previous genetic and biochemical data and highlight the mechanisms driving eukaryotic ribosome assembly in a unidirectional manner.

The assembly of the large eukaryotic ribosomal subunit (60S) is organized as a series of consecutive intermediates, which are regulated by different sets of ribosome assembly factors in the nucleolus, nucleus, and cytoplasm[1]. During the past decade, three major types of pre-60S particles have been observed, each with a distinct composition of assembly factors, representing late nucleolar[2], nuclear[3] and late nucleo-cytoplasmic intermediates[4]. The earliest pre-60S particles exist in the nucleolus, where they undergo major RNA processing steps and conformational changes. Subsequently, in the nucleoplasm, the internal transcribed spacer 2 (ITS2) RNA is removed and the particles are assembled into a nuclear export competent state. Exported particles then complete the final steps of maturation in the cytoplasm.

While previous high-resolution structural studies have revealed the architectures of the late nucleolar and export-competent pre-60S particles, the early nucleolar particles, containing specific factors such as Nsa1 have so far remained elusive[2,4]. Although the identities and approximate binding regions of many early nucleolar ribosome assembly factors are known, their structures and functions have not yet been determined[5].

To elucidate the mechanisms that govern early nucleolar large subunit assembly, several laboratories, including ours, have observed that cellular starvation elongates the lifetime of a 27SB pre-rRNA containing species[6,7]. Here, we have isolated these intermediates from starved yeast by employing a tandem affinity purification involving tagged ribosome assembly factors Nsa1 and Nop2 (Extended Data Fig. 1). Similar to the small subunit processome, the nucleolar pre-60S particle, which is compositionally related to Nsa1-containing particles[8], accumulates upon starvation. Purified nucleolar pre-60S particles were analyzed by cryo-EM leading to the discovery of a high-resolution core (3.4 Å) that was further sub-classified into three states, which were determined at resolutions of 4.3 Å (state 1), 3.7 Å (state 2) and 4.6 Å (state 3) (Table 1 and Extended Data Figs. 2, 3). These three states, together with cross-linking and mass spectrometry data, resulted in the identification of 21 ribosome assembly factors (Extended Data Table 1 and Supplementary Data Set 1). Atomic models could be completed for 18 of these proteins, while homology and poly-alanine models were used for proteins such as Ebp2, Mak11, and Ytm1, which were located in more flexible regions (Fig. 1, Extended Data Fig. 4).

The purified pre-60S particles contain 27SB rRNA that has not yet been processed at ITS2 (Extended Data Fig. 1). We observed three different conformational states of this RNA (Extended Data Figs. 2 and 5). State 1 includes ordered density for ITS2 and domains I, II and the 5.8S rRNA. State 2 additionally revealed density for domain VI, which is present in a near-mature conformation. In contrast to state 2, state 3 lacks an ordered domain VI but features domain III. Although present, the majority of domains IV, V and the 5S RNP were poorly resolved in all of the reconstructions, due to conformational flexibility. Low-resolution features corresponding to parts of domain V (helices 74–79) and its proximal assembly factor Mak11 can be seen in states 2 and 2A (Fig. 1, Extended Data Fig. 2).

A striking feature of the nucleolar pre-60S particle is its open architecture where the solvent-exposed domains I, II and VI are encapsulated by a series of ribosome assembly factors as visualized in state 2 (Fig.1, Extended Data Fig. 5 and Supplementary Video). Interestingly, ribosomal proteins that have been associated with Diamond Blackfan anemia[9] are located at critical rRNA domain interfaces in the structure (Extended Data Fig. 6), suggesting that their architectural roles are especially important during early nucleolar assembly, where defects can trigger the nucleolar stress response.

Domains I, II and VI adopt an open conformation that is chaperoned by eight early ribosome assembly factors, which form a ring-like structure at the solvent-exposed side (Fig. 2a). In particular, Brix-domain containing factors (Brx1, Rpf1 and Ssf1) act in conjunction with their respective binding partners (Ebp2, Mak16 and Rrp15) to interconnect these junctions and sterically prevent premature RNA-protein and RNA-RNA contacts. Architectural support for the major interface between domains I and II is provided by Rpf1 and its zinc-binding interaction partner Mak16, the helical repeat protein Rrp1 and the beta-propeller Nsa1. Rpf1 and Nsa1 occupy a region near the domain I binding site of Rpl17, while Mak16 and Rrp1 interface predominantly with ribosomal proteins Rpl4 and Rpl32 within domain II (Fig. 2b).

The ring-like structure encapsulating domains I, II and VI is continued in one direction by the Ssf1•Rrp15 heterodimer and Rrp14. While the long C-terminal helix of Rrp14 bridges domains II and VI, the Ssf1•Rrp15 complex is positioned at the interface of domains I and

[1]equal contribution. [2]Laboratory of Protein and Nucleic Acid Chemistry, The Rockefeller University, New York, New York 10065, USA. [3]Tri-Institutional Training Program in Chemical Biology, The Rockefeller University, New York, New York 10065, USA. [4]Laboratory of Mass Spectrometry and Gaseous Ion Chemistry, The Rockefeller University, New York, New York 10065, USA.

VI (Fig. 2a). Here, Ssf1 occupies the same position as Rpl31, which in the later Nog2-containing pre-60S particles binds at the interface of domains III and VI near the polypeptide exit tunnel (PET)[2]. The PET, which is created by domains I, III and VI at the solvent exposed side, is already formed in the Nog2 particle, where it is blocked by the C-terminal domain (CTD) of the GTPase Nog1 (Fig. 2c, d).

The role of the Brx1•Ebp2 heterodimer near the interface of domains I and II is two-fold. While being involved in the stabilization of these domains, its strategic binding site prevents the premature assembly of the large subunit (LSU) by steric hindrance. In later stages of LSU assembly, an RNA segment of domain I (helix 22) base-pairs with a region in domain V (helix 88) near a separate region of domain IV (helix 68) (Fig. 2e, f). Brx1 remodels helix 22 of domain I to block the premature formation of this tertiary structure with helix 88. Similarly, Brx1 prevents the mature conformations of domain IV (helix 68), domain II (expansion segment 9) and the C-terminal region of Rpl13 in this region (Fig. 2e, f).

In state 3, we have identified the Erb1•Ytm1 heterodimer bound to domain III via Rpl27 (Fig. 3a). The N-terminal region of Erb1 (residues 239–397) wraps around the entire ITS2-domain I interface and is positioned underneath Nop16 and Has1 (Fig. 3b, c). This location is in agreement with previous cross-linking data and explains why deletions within this region prevent the incorporation of Erb1 into pre-60S particles[10,11]. Nop16 interconnects RNA elements of the 5.8S rRNA and regions of domain I, and additionally contains a bipartite binding site by interacting with ribosomal proteins Rpl8 and Rpl13 (Fig. 3c). The DEAD-box helicase Has1 is positioned at the interface of Rpl8, Cic1, Nop16 and Erb1 (Fig. 3c). Assembly factors Cic1, Rlp7, Nop7 and Nop15 appear both in the nucleolar pre-60S particle and the Nog2-particle in largely the same conformation (Fig. 3c, d).

Strikingly, the N-terminal segment of Erb1 employs molecular mimicry by binding to Nop7 in a similar fashion as Nop53 in the Nog2-particle, which uses a structurally related motif to bind to Nop7. This steric hindrance is exacerbated by the alternate conformation of the N-terminus of Rlp7 that further prevents Nop53 binding (Fig. 3e, f). Therefore, the coordinated mechanical removal of Erb1 and its proximal factors Ytm1, Nop16 and Has1 by Mdn1 is required before Nop53 can bind to the Nog2-particle and recruit the exosome-associated RNA helicase Mtr4 for ITS2 processing[12,13]. The Has1 helicase may have acted upon its substrate at an earlier stage during the 27SA3 to 27SB transition. Alternatively, it may remodel flexible RNA elements in its vicinity for the ensuing 27SB processing[14].

The nucleolar pre-60S states 2 and 3 represent distinct assembly intermediates of the polypeptide exit tunnel (Fig. 4). Ssf1, Rrp15 and Rrp14 are ordered in state 2 where they chaperone domains I and VI, that line two sides of the forming polypeptide exit tunnel (PET) (Fig. 2b, c). By contrast, domain VI, Ssf1, Rrp15 and Rrp14 are disordered in state 3. Here, Ytm1 and Erb1 chaperone domain III, which adopts a mature conformation with respect to domain I to form a different intermediate of the PET (Fig. 3a, b). A subsequent maturation step of states 2 and 3 likely involves the joining of domains III and VI and the formation of the PET on the solvent exposed side. This may be accompanied by the insertion of the Nog1 N-terminus into the nascent PET and the replacement of Ssf1•Rrp15 by Rpl31 (Figs. 2c, d and 4).

Conformational changes first by the initially flexible domain V/5S RNP together with the Nog1 GTPase domain and subsequently domain IV will result in the overall conformation observed in the late-nucleolar Nog2-particle[2] (Figs. 2c, d and 4). The base-pairing between domains I and V will be possible upon the dissociation of the Brx1•Ebp2 complex (Fig. 2e, f), while the release of Rrp1, Rpf1 and Mak16 is likely brought about by the ATPase Rix7 acting upon the proximal Nsa1 (ref. 15). In the ITS2 region, Mdn1-dependent removal of Erb1•Ytm1 will expose the binding site of Nop53 and may also trigger the exit of Nop16 and Has1 from the particle[13].

While this manuscript was under review, complementary structural data on the nucleolar assembly of the large ribosomal subunit was published[16]. Differences in purification conditions have resulted in the isolation of distinct states, which may either represent assembly stages or breakdown products. These data now enable the visualization of early nucleolar pre-60S intermediates from the formation of the solvent exposed side of the particle to the incorporation of the DEAD-box helicase Spb4 at the subunit interface (Extended Data Fig. 7). Throughout the assembly, proteins such as Erb1, Brx1 and later Spb1 use steric hindrance to prevent the premature association of subsequent maturation factors (Extended Data Fig. 8). Additionally, flexible elements of Ebp2 and Erb1 are employed to reduce conformational freedom of the maturing particles.

Eukaryotic nucleolar 60S ribosome assembly is conceptually reminiscent of the early prokaryotic 50S assembly intermediates where different rRNA domains are assembled in a modular fashion[17] (Fig. 4 and Extended Data Fig. 7). However, our structures of nucleolar pre-60S particles highlight the high degree of control that is exerted to prevent the premature formation of inter-domain contacts of ribosomal RNA. They further illustrate how the reduction of conformational freedom and a chronology of assembly factors are enforced during assembly. These overarching themes exist for the nucleolar stages of both small and large ribosomal subunit assembly[18].

Online Content Methods, along with any additional Extended Data display items and Source Data, are available in the online version of the paper; references unique to these sections appear only in the online paper.

Received 30 November 2017; accepted 23 February 2018.
Published online 5 March 2018.

1. Konikkat, S. & Woolford, J. L. Principles of 60S ribosomal subunit assembly emerging from recent studies in yeast. *Biochem. J.* **474**, 195–214 (2017).
2. Wu, S. *et al.* Diverse roles of assembly factors revealed by structures of late nuclear pre-60S ribosomes. *Nature* **534**, 133–137 (2016).
3. Barrio-Garcia, C. *et al.* Architecture of the Rix1-Rea1 checkpoint machinery during pre-60S-ribosome remodeling. *Nat. Struct. Mol. Biol.* **23**, 37–43 (2015)
4. Ma, C. *et al.* Structural snapshot of cytoplasmic pre-60S ribosomal particles bound by Nmd3, Lsg1, Tif6 and Reh1. *Nat. Struct. Mol. Biol.* **24**, 214–220 (2017).
5. Chen, W., Xie, Z., Yang, F. & Ye, K. Stepwise assembly of the earliest precursors of large ribosomal subunits in yeast. *Nucleic Acids Research* **45**, 6837–6847 (2017).
6. Talkish, J. *et al.* Disruption of ribosome assembly in yeast blocks cotranscriptional pre-rRNA processing and affects the global hierarchy of ribosome biogenesis. *RNA* **22**, 852–866 (2016).
7. Kos-Braun, I. C., Jung, I. & Koš, M. Tor1 and CK2 kinases control a switch between alternative ribosome biogenesis pathways in a growth-dependent manner. *PLoS Biol* **15**, e2000245 (2017).
8. Harnpicharnchai, P. *et al.* Composition and functional characterization of yeast 66S ribosome assembly intermediates. *Mol. Cell* **8**, 505–515 (2001).
9. Adam, M. P. *et al.* Diamond-Blackfan Anemia. (1993).
10. Granneman, S., Petfalski, E. & Tollervey, D. A cluster of ribosome synthesis factors regulate pre-rRNA folding and 5.8S rRNA maturation by the Rat1 exonuclease. *EMBO J* **30**, 4006–4019 (2011).
11. Konikkat, S., Biedka, S. & Woolford, J. L. The assembly factor Erb1 functions in multiple remodeling events during 60S ribosomal subunit assembly in *S. cerevisiae*. *Nucleic Acids Research* **45**, 4853–4865 (2017).
12. Thoms, M. *et al.* The Exosome Is Recruited to RNA Substrates through Specific Adaptor Proteins. *Cell* **162**, 1029–1038 (2015).
13. Bassler, J. *et al.* The AAA-ATPase Rea1 Drives Removal of Biogenesis Factors during Multiple Stages of 60S Ribosome Assembly. *Mol Cell* **38**, 712–721 (2010).
14. Dembowski, J. A., Kuo, B. & Woolford, J. L. Has1 regulates consecutive maturation and processing steps for assembly of 60S ribosomal subunits. *Nucleic Acids Research* **41**, 7889–7904 (2013).
15. Kressler, D., Roser, D., Pertschy, B. & Hurt, E. The AAA ATPase Rix7 powers progression of ribosome biogenesis by stripping Nsa1 from pre-60S particles. *The Journal of Cell Biology* **181**, 935–944 (2008).
16. Kater, L. *et al.* Visualizing the Assembly Pathway of Nucleolar Pre-60S Ribosomes. *Cell* **171**, 1599–1610.e14 (2017).
17. Davis, J. H. *et al.* Modular Assembly of the Bacterial Large Ribosomal Subunit. *Cell* **167**, 1610–1622.e15 (2016).
18. Barandun, J. *et al.* The complete structure of the small-subunit processome. *Nat. Struct. Mol. Biol.* **24**, 944–953 (2017).

Supplementary Information is available in the online version of the paper.

Acknowledgements We thank M. Ebrahim and J. Sotiris for their outstanding support with data collection at the Evelyn Gruss Lipper Cryo-EM resource center, M. Tesic-Mark for analysis of mass spectrometry data, and C. Cheng for help with the initial manual curation and analysis of the nucleolar pre-60S particles. We further thank the Walz lab for helpful discussions. L.M. is supported in part by NIH T32 GM115327-Tan. J.B. is supported by an EMBO long-term fellowship (ALTF 51–2014) and a Swiss National Science Foundation fellowship (155515). M.C.-M. is supported by a postgraduate scholarship from NSERC. S.K. is supported by the Robertson Foundation, the Irma T. Hirschl Trust, the Alexandrine and Alexander L. Sinsheimer Fund, the Rita Allen Foundation, and an NIH New Innovator Award (1DP2GM123459). B.T.C. is supported by National Institute of Health Grant Nos. P41GM103314 and P41GM109824.

Author Contributions S.K. and Z.S. established purification conditions. Z.S., L.M., and S.K. determined the cryo-EM structure of the yeast nucleolar pre-60S particle. K.R.M., J.W., and B.T.C. processed and analyzed DSS cross-linking data. Z.S., L.M., J.B., M.C.-M., M.H., and S.K. built the model, L.M. performed all RNA work, and Z.S., L.M., J.B., M.H., M.C.-M., and S.K. interpreted the results and wrote the manuscript.

Author Information Reprints and permissions information is available at www.nature.com/reprints. The authors declare no competing interests. Readers are welcome to comment on the online version of the paper. Publisher's note: Springer Nature remains neutral with regard to jurisdictional claims in published maps and institutional affiliations. Correspondence and requests for materials should be addressed to S.K. (klinge@rockefeller.edu).

Reviewer Information *Nature* thanks A. Amunts, D. Tollervey and J. Woolford for their contribution to the peer review of this work.

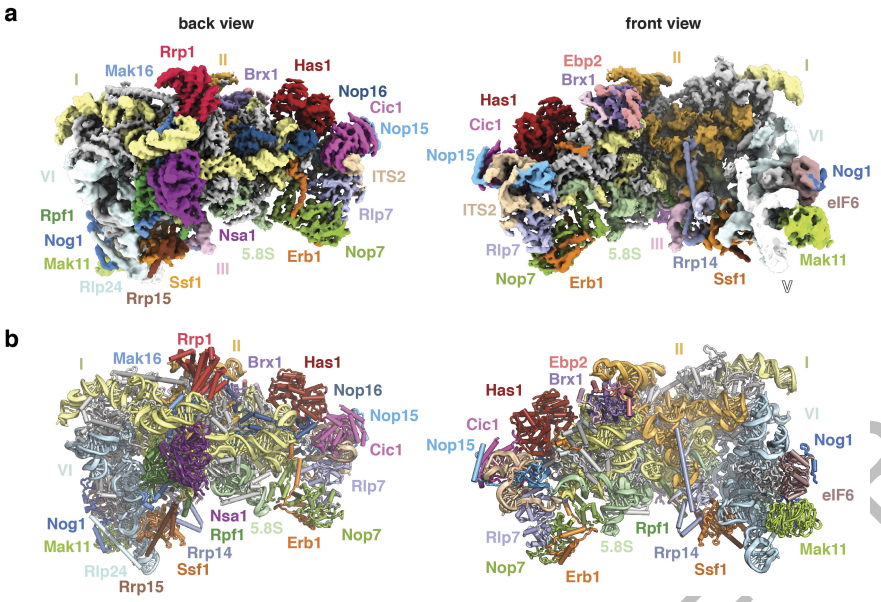

Figure 1 | Structure of the early nucleolar pre-60S particle. (**a**) Composite cryo-electron density map of state 2 consisting of 25S rRNA domains I and II (3.4 Å) and VI (3.7 Å) (low-pass filtered to 5 Å) and associated proteins. (**b**) Corresponding near-atomic model of state 2 with ribosome assembly factors and 25S rRNA domains labeled and color-coded. Ribosomal proteins are shown in grey.

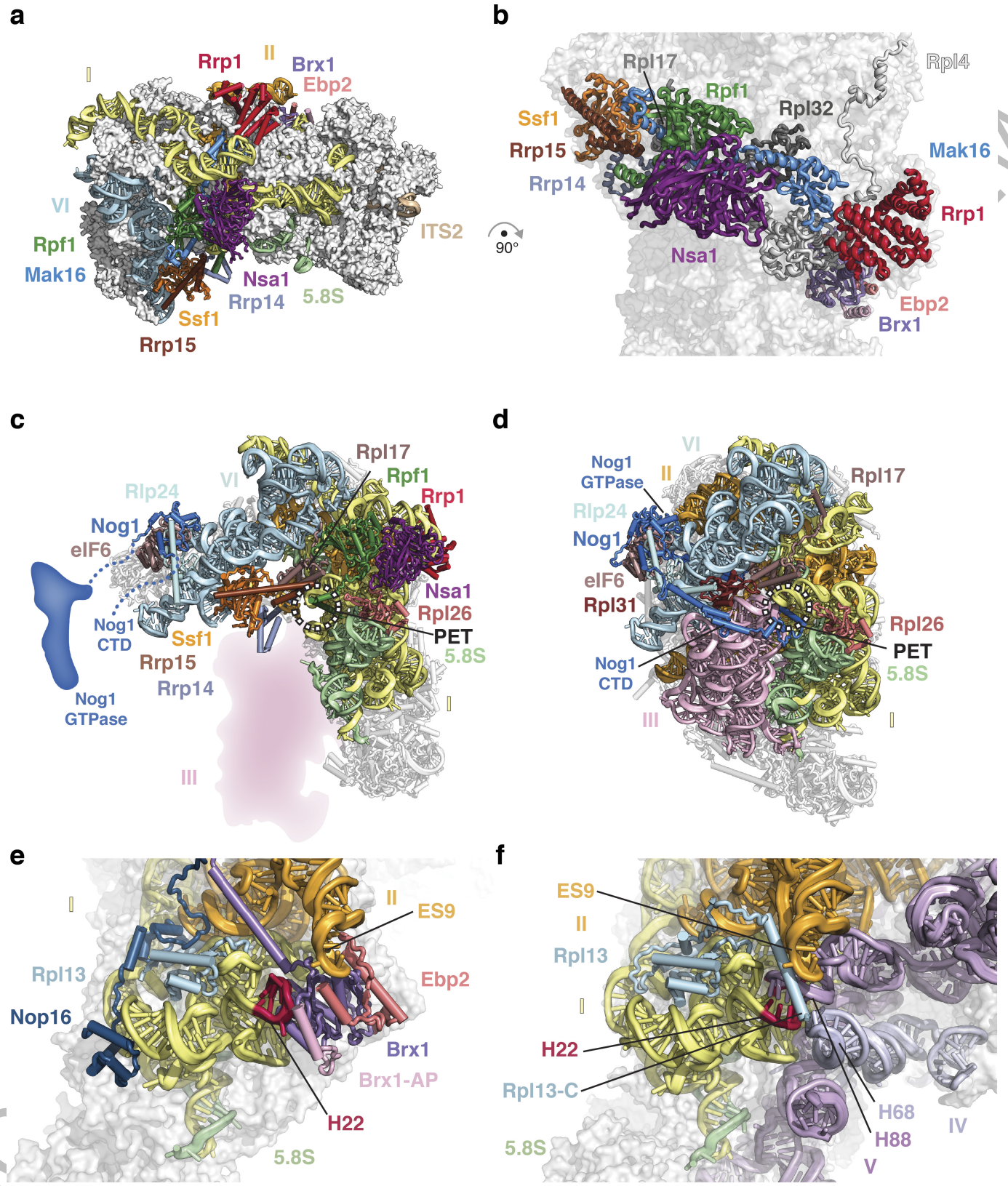

Figure 2 | A ring of nucleolar assembly factors prevents premature folding of the 25S rRNA. (**a**, **b**) Assembly factors chaperone areas of domains I, II and VI and interact with ribosomal proteins. (**c**, **d**) Assembly factors prevent the formation of the polypeptide exit tunnel (PET). (**c**) In state 2, Ssf1•Rrp15 block the binding of Rpl31. Nog1 is largely unstructured. (**d**) In the Nog2-particle (PDB 3JCT), the PET is formed, probed by Nog1 and supported by Rpl31. (**e**, **f**) Brx1•Ebp2 and an associated peptide (Brx1-AP) remodel domain I (helix 22) to prevent binding of domain V (helix 88) and domain IV (helix 68) (**e**). These interactions exist in the Nog2-particle (**f**).

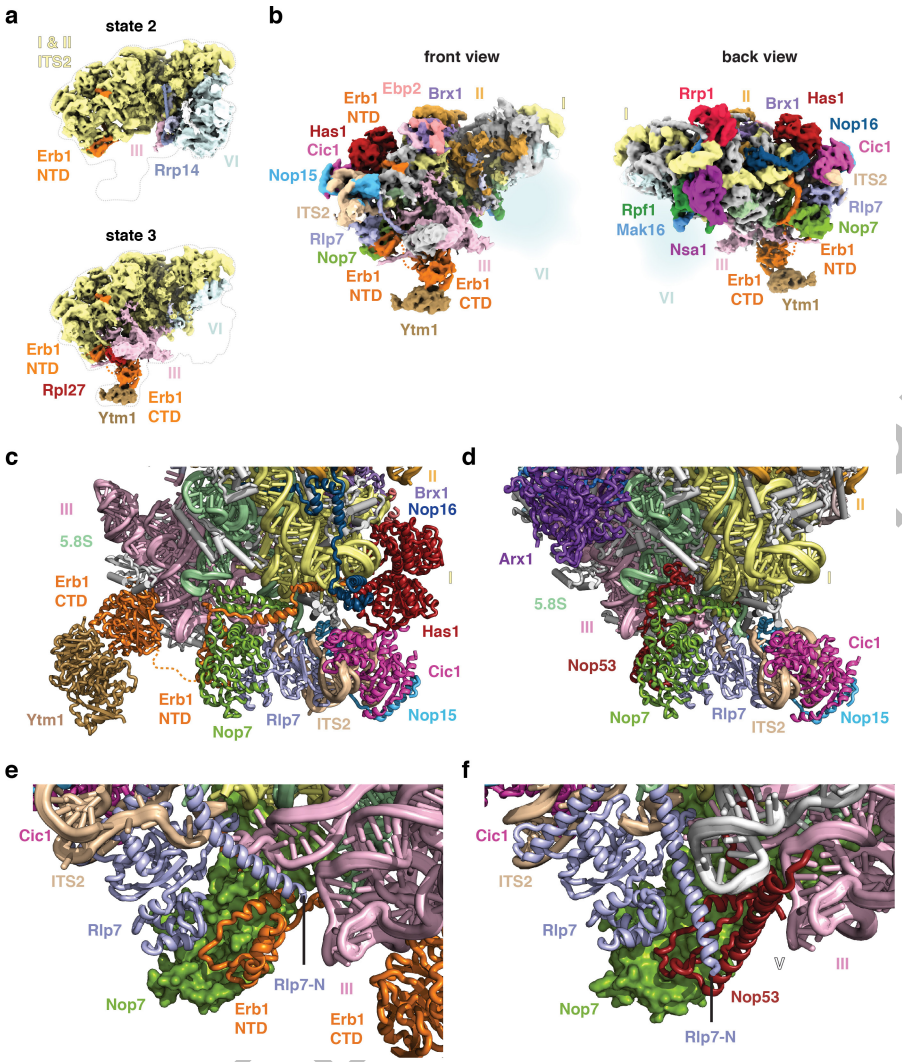

Figure 3 | Molecular mimicry by Erb1 prevents premature ITS2 processing. (**a**) Cryo-EM maps of states 2 and 3 of the nucleolar pre-60S particle. State 2 contains domain VI but limited density for domain III, while state 3 contains domain III with a flexible domain VI. (**b**) Two views of the state 3 cryo-EM map. (**c**, **d**) Cartoon representation of the ITS2 region in state 3 of the nucleolar pre-60S particle (**c**) and the Nog2-particle (PDB 3JCT) (**d**). (**e**, **f**) The N-termini of Erb1 and Rlp7 in the nucleolar pre-60S particle prevent the binding of Nop53 (**e**), which binds to Nop7 in the Nog2-particle (**f**).

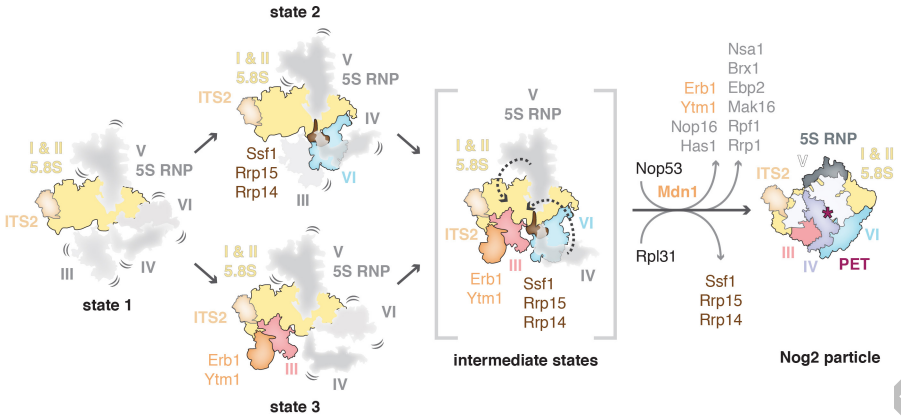

Figure 4 | Model for early nucleolar stages of large subunit assembly. Domains of the 25S rRNA are represented as separate segments that are flexible (in grey) or stably incorporated (in color). State 1 represents an intermediate in which domains I and II are ordered and subsequent folding of either domain III or VI will occur (state 3 and state 2, respectively) to partially form the polypeptide exit tunnel (PET). To mature into the Nog2-particle, the formation of the nascent PET must occur by Mdn1 and Rix7-dependent exchange and removal of assembly factors alongside the stepwise folding of domain V followed by domain IV.

Table 1 | Cryo-EM data collection parameters and refinement and validation statistics

	core	state 2 EMD-7324 PDB 6C0F	state 2A	state 3 EMD-7445 PDB 6CB1
Data collection and processing				
Magnification	22,500X			
Voltage (kV)	300			
Pixel size (Å)	1.3			
Electron exposure (e-/Å^2)	47			
Defocus range (um)	1.0–3.5			
Symmetry imposed	C1			
Initial particle images	1,653,290			
Final particle images	514,746	201,114	75,512	31,419
Resolution (Å)	3.4	3.7	4.2	4.6
FSC threshold	0.143			
Map sharpening B-Factor (Å^2)	-68.7	-71.7	-83.0	-94.2
Refinement				
Model composition				
Non hydrogen atoms		91,741		69,945
Protein residues		7197		6347
RNA bases		1602		1615
Ligands		3		2
R.m.s. deviations				
Bond length (Å)		0.007		0.006
Angles (°)		1.11		1.10
Validation				
MolProbity score		1.91		1.68
Clashscore		10.67		5.96
Rotamer outliers (%)		0.30		0.13
Good sugar puckers (%)		98		97
Ramachandran				
Favored (%)		94.75		94.85
Allowed (%)		5.18		5.02
Outliers (%)		0.07		0.13

METHODS

Purification of nucleolar pre-60S particles. Nucleolar pre-60S particles were purified from a *Saccharomyces cerevisiae* BY4741 strain containing a TEV protease-cleavable C-terminal GFP tag on Nsa1 (Nsa1-40aaLinker-TEV-GFP) and a C-terminal 5 x beta-catenin 3C protease-cleavable tag on Nop2 (Nop2-40aaLinker-3C-Bc5), for endogenous expression. Cultures were grown in full synthetic drop-out (SD) media containing 2% raffinose (w/v) at 30 °C to an optical density (OD) of 0.8–1, prior to addition of 2% galactose (w/v) for 16 h, reaching saturation (OD 5–6). Cells were then harvested by centrifugation at 3000 × *g* for 10 min at 4 °C. The cell pellet was washed with ice-cold ddH_2O twice, followed by a wash with ddH_2O containing protease inhibitors (E64, Pepstatin, PMSF). Washed cells were immediately flash frozen in liquid nitrogen and lysed by 4 cycles of cryogenic grinding using a Retsch Planetary Ball Mill PM100.

The freshly ground yeast powder was resuspended by vortexing in buffer A (50 mM Tris-HCl, pH 7.6 (20 °C), 150 mM NaCl, 1 mM EDTA, 1 mM DTT, 0.1% Triton-X100, PMSF, Pepstatin, E-64). The insoluble fraction was removed by centrifugation at 4 °C, 40,000 × *g* for 30 min. The supernatant was subsequently incubated with anti-GFP nanobody beads (Chromotek) for 3 h at 4 °C, with agitation. The beads were washed four times in ice-cold buffer A before the bound proteins were eluted via TEV-protease cleavage (1 h, 4 °C). The eluate was then incubated with NHS-sepharose beads (Sigma) coupled with anti-beta-catenin nanobody[23] in buffer B (50 mM Tris-HCl pH 7.6 (20 °C), 150 mM NaCl, 1 mM EDTA, 1 mM DTT) for 1 h at 4 °C with agitation. For electron microscopy (EM) sample preparation, the anti-beta catenin beads were washed once with buffer B. Cleavage by 3C protease for 1 h at 4 °C released the Nsa1-Nop2 containing nucleolar pre-60S particles. For protein-protein cross-linking analysis the eluate from GFP-nanobody beads was incubated with beta catenin-nanobody beads in buffer C (50 mM HEPES-NaOH pH 7.6 (4 °C), 150 mM NaCl, 1 mM EDTA) and eluted in the same buffer through 3C-protease cleavage. The eluate typically measured an absorbance at 260 nm (A260) of 2.4 to 4.5 mAU (Nanodrop 2000, Thermo Scientific) (Extended Data Fig. 1).

Cryo-EM sample and grid preparation. Cryo-EM grids were prepared on four different occasions for the 4 data sets obtained (ds1-ds4). The nucleolar pre-60S particle eluate in sample buffer B (above) was left as is (ds1 only), or supplemented with 0.1% Triton X-100 and 5 mM $MgCl_2$ (final concentration, ds2-ds4). Copper grids of 400 mesh with lacey carbon and an ultra-thin carbon support film were used (Ted Pella Inc., product no. 01824) for data collection. A volume of 3 to 4 µl of nucleolar pre-60S particle sample (absorbance at 260 nm of 2.5) was applied onto glow-discharged grids and plunged into liquid ethane using a Vitrobot Mark IV robot (FEI Company) (100% humidity, blot force of 0 and blot time 3.5–4 s).

Cryo-EM data collection and image processing. A total of 14,201 micrographs were obtained over four data collections (ds1 - ds4) on a Titan Krios (FEI Company), at 300 kV, with a K2 Summit detector (Gatan, Inc.). SerialEM[24] was employed for data acquisition using a defocus range of 1.0–3.5 µm with a pixel size of 1.3 Å. Super-resolution movies with 32 frames were collected using a total dose of 10 electrons per pixel per second with an exposure time of 8 seconds and a total dose of 47 electrons per $Å^2$ (Table 1).

Upon data collection, the movies were gain corrected, dose weighted and aligned with Motioncor2 (ref. 20), and the contrast transfer function (CTF) was estimated using CTFFIND 4.1.5 (ref. 25). Relion 2.1 (ref. 21) was used for all subsequent particle picking, classifications and refinements. Corrected and aligned micrographs were first subjected to autopicking in Relion, resulting in a total of 1,653,290 selected particles from all 4 data sets. After manual inspection of all micrographs, particles were extracted with a box size of 480 pixels (2X-binned to 240 pixels), and 2D-classified separately for each individual data set. After 2D classification, bad classes were removed, and the selected particles of each data set were 3D-classified into four classes using an initial 3D model obtained from cryoSPARC[26], low-pass filtered to 60 Å. The best one to two classes from each 3D classification were selected and their particles were re-extracted with a box size of 480 pixels (un-binned). A combined total of 514,746 particles were finally used for 3D auto-refinement and post-processing with a solvent mask around a "core" containing domains I and II of the 25S rRNA, resulting in an overall resolution of 3.4 Å (Extended Data Fig. 2, 3a). Since the more flexible domains III-VI were not visible in this state due to averaging of different populations, a subsequent round of 3D classification without image alignment of these particles into 6 classes was used to obtain the two classes that contained states 2 (39%) and states 1 and 3 (41%). A refinement of the class containing state 2 (201,114 particles) was performed using a mask to include the additional visible densities, comprising of domain VI and its associated proteins, to obtain a final map at 3.7 Å (Extended Data Fig. 2, 3b). By conducting an additional round of focused 3D classification without image alignment on this class with a mask around Mak11 and the neighboring segment of domain V of the 25S rRNA, a subset of particles (36%) emerged with improved density. This was refined to provide a more continuous map of Mak11 and domain V (state 2A) (Extended Data Fig. 2, 3c). The remaining 64% of particles did not reveal additional features beyond those seen in state 2.

Due to particle heterogeneity in the initial class containing states 1 and 3 (41%, 211,534 particles), a focused classification without image alignment of that class of particles was performed using a mask around the additional density containing domain III of the 25S rRNA, Erb1-CTD (WD40) and Ytm1 (WD40). The class from this round of classification containing density for domain III (31,419 particles) was refined with a mask around the entirety of state 3, to obtain a final map at 4.6 Å resolution (Extended Data Fig. 2, 3d). The highest resolution class of particles from this classification, which contained no density for domain III (126,824 particles), was refined to obtain the 4.3 Å map of state 1. The map of state 1 closely resembles the higher resolution core map (correlation coefficient= 0.96). The local resolution of the maps were calculated using Resmap[22] (Extended Data Fig. 3).

Model building and refinement. By using the structure of the late nucleolar pre-60S particle, the Nog2-particle (PDB 3JCT)[2] as reference, common assembly factors and ribosomal proteins were manually located and fitted into the density, using Cic1 and Rpl7 as hallmark anchors. Protein identification and tracing were aided by crosslinking and mass spectrometry analyses (described below). New assembly factors Mak16, Rrp1, Nop16, Erb1-NTD, Rrp14, Rrp15 and Ebp2 and segments of rRNA were modeled *de novo*. Previously determined crystal structures of assembly factors Nsa1 (PDB 5SUI)[27], Ytm1 (PDB 5CXB), Erb1-CTD (PDB 4U7A)[28] were docked and manually adjusted. Has1, Ssf1, Brx1, Rpf1 and Mak11 were docked from Phyre2 models[29] initially and manually built to fit the density. Model building was performed with COOT[30]. An annotated list of individual protein IDs, reference models and corresponding maps used for building, can be found in Extended Data Table 1. The model was refined against a half-map1 from the overall 3.7 Å map of state 2 in PHENIX with phenix.real_space_refine using secondary structure restraints for proteins and RNAs[31]. Refinement and model statistics can be found in Table 1.

Map and model visualization. All map and model analyses and illustrations were made using Chimera[32] and PyMOL Molecular Graphics System, Version 1.8 Schrödinger, LLC. Density map visualization for certain figures was also performed on UCSF ChimeraX, developed by the Resource for Biocomputing, Visualization, and Informatics and the University of California, San Francisco (supported by NIGMS P41-GM103311).

RNA extraction and Northern blotting. The *S. cerevisiae* nucleolar pre-60S particle (Nsa1/Nop2 particle) was purified as described above and RNA was extracted from the final 3C-protease elution with 1 mL TRIzol (Life Technologies) according to the manufacturer's instructions. 1.0 µg of isolated nucleolar pre-60S RNA was separated on a denaturing 1.2% formaldehyde-agarose gel (SeaKem LE, Lonza) or on a denaturing 10% Urea-PAGE (Fisher, Amresco) for the 5S rRNA Northern blot. After staining the gel in 1X SYBR Green II (Lonza) ddH_2O solution (pH 7.5) for 30 min, RNA species were visualized with a Gel Doc EZ Imager (Bio-Rad) (Extended Data Fig. 1d, e) and then transferred onto a cationized nylon membrane (Zeta-Probe GT, Bio-Rad) using downward capillary transfer for the agarose gel and a Trans Blot SD semi-dry transfer cell (Bio-Rad) for the Urea-PAGE gel. RNA was cross-linked to the membrane for Northern blot analysis by UV irradiation at 254 nm with a total exposure of 120 millijoules/cm^2 in a UV Stratalinker 2400 (Stratagene). Cross-linked membranes were incubated with hybridization buffer (750 mM NaCl, 75 mM trisodium citrate, 1% (w/v) SDS, 10% (w/v) dextran sulfate, 25% (v/v) formamide) at 65 °C for 30 min prior to addition of γ-^{32}P-end-labeled DNA oligo nucleotide probes. Used oligonucleotide probe sequences are as follows:
25S (TTTCACTCTCTTTTCAAAGTTCTTTTCATCT),
the ITS1 3' end (TTAATATTTTAAAATTTCCAG),
the ITS2 C2 site (TGGTAAAACCTAAAACGACCGT),
the 3' ETS 5' end (CCACTTAGAAAGAAATAAAAA),
and the 5S (CTACTCGGTCAGGCTC).

Probes were hybridized for 1 h at 65 °C and then overnight at 37 °C. Membranes were washed once with wash buffer 1 (300 mM NaCl, 30 mM trisodium citrate, 1% (w/v) SDS) and once with wash buffer 2 (30 mM NaCl, 3 mM trisodium citrate, 1% (w/v) SDS) for 20 min each at 45 °C. Radioactive signal was detected by exposure of the washed membranes to a storage phosphor screen which was scanned with a Typhoon 9400 variable-mode imager (GE Healthcare). For Northern blot source data, see Supplementary Figure 1.

DSS cross-linking sample preparation and mass spectrometry analysis. The tandem-affinity purified nucleolar pre-60S particles (Nsa1/Nog2-particle), eluted off of anti-beta catenin nanobody beads (in 50 mM HEPES-NaOH pH 7.6 (4 °C), 150 mM NaCl, 1 mM EDTA, 1 mM DTT) at an absorbance of 1.0 at 260 nm (Nanodrop 2000, Thermo Scientific) were pooled (total volume 300 µl) and split into three 100 µl cross-linking reaction aliquots.

Disuccinimidylsuberate (DSS; 25 mM in DMSO, Creative Molecules Inc.) was added to each aliquot to yield a final DSS concentration of 2.0 mM and samples

were cross-linked for 30 min at 25 °C with 450 rpm constant mixing. The reactions were quenched with 50 mM ammonium bicarbonate (final concentration) and precipitated by adding methanol (Alfa Aesar, LC-MS grade) to a final concentration of 90% followed by incubation at −80 °C overnight. Precipitated cross-linked nucleolar pre-60S particles were combined into one tube by repeated centrifugation at 21,000 × *g*, 4 °C for 30 min. The resulting pellet was washed three times with 1 ml ice-cold 90% methanol, air-dried and finally resuspended in 50 µl of 1X NuPAGE LDS buffer (Thermo Fisher Scientific).

DSS cross-linked samples were processed as in[18], and as described below. DSS cross-linked nucleolar pre-60S particle in LDS buffer were reduced with 25 mM DTT, alkylated with 100 mM 2-chloroacetamide, separated by SDS-PAGE in three lanes of a 3–8% Tris-Acetate gel (NuPAGE, Thermo Fisher Scientific), and stained with Coomassie-blue. The gel region corresponding to cross-linked complexes was sliced and digested overnight with trypsin to generate cross-linked peptides. After digestion, the peptide mixture was acidified and extracted from the gel as previously described[33,34]. Peptides were fractionated offline by high pH reverse-phase chromatography, loaded onto an EASY-Spray column (Thermo Fisher Scientific ES800: 15 cm × 75 µm ID, PepMap C18, 3 µm) via an EASY-nLC 1000, and gradient-eluted for online ESI-MS and MS/MS analyses with a Q Exactive Plus mass spectrometer (Thermo Fisher Scientific). MS/MS analyses of the top 8 precursors in each full scan used the following parameters: resolution: 17,500 (at 200 Th); AGC target: 2×10^5; maximum injection time: 800 ms; isolation width: 1.4 m/z; normalized collision energy: 24%; charge: 3–7; intensity threshold: 2.5×10^3; peptide match: off; dynamic exclusion tolerance: 1,500 mmu. Cross-linked peptides were identified from mass spectra by pLink[35]. All spectra reported here were manually verified as previously[33].

Data availability. Cryo-EM density maps for the yeast nucleolar pre-60S particle states 2 and 3 have been deposited in the EM Data Bank with accession codes EMD-7324 and EMD-7445 respectively. Atomic coordinates for the yeast nucleolar pre-60S particle states 2 and 3 have been deposited in the Protein Data Bank under accession codes 6C0F and 6CB1 respectively. A PyMOL session for the analysis of the yeast nucleolar pre-60S particle in state 2 is available in Supplementary Data Set 2.

19. Bradatsch, B. *et al.* Structure of the pre-60S ribosomal subunit with nuclear export factor Arx1 bound at the exit tunnel. *Nat. Struct. Mol. Biol.* **19**, 1234–1241 (2012).
20. Zheng, S. Q. *et al.* MotionCor2: anisotropic correction of beam-induced motion for improved cryo-electron microscopy. *Nat. Methods* **14**, 331–332 (2017).
21. Kimanius, D., Forsberg, B. O., Scheres, S. H. & Lindahl, E. Accelerated cryo-EM structure determination with parallelisation using GPUs in RELION-2. *Elife* **5**, 19 (2016).
22. Kucukelbir, A., Sigworth, F. J. & Tagare, H. D. Quantifying the local resolution of cryo-EM density maps. *Nat. Methods* **11**, 63–65 (2014).
23. Braun, M. B. *et al.* Peptides in headlock--a novel high-affinity and versatile peptide-binding nanobody for proteomics and microscopy. *Sci Rep* **6**, 19211 (2016).
24. Mastronarde, D. N. Automated electron microscope tomography using robust prediction of specimen movements. *J. Struct. Biol.* **152**, 36–51 (2005).
25. Rohou, A. & Grigorieff, N. CTFFIND4: Fast and accurate defocus estimation from electron micrographs. *J. Struct. Biol.* **192**, 216–221 (2015).
26. Punjani, A., Rubinstein, J. L., Fleet, D. J. & Brubaker, M. A. cryoSPARC: algorithms for rapid unsupervised cryo-EM structure determination. *Nat. Methods* **14**, 290–296 (2017).
27. Lo, Y.-H., Romes, E. M., Pillon, M. C., Sobhany, M. & Stanley, R. E. Structural Analysis Reveals Features of Ribosome Assembly Factor Nsa1/WDR74 Important for Localization and Interaction with Rix7/NVL2. *Structure* **25**, 762–772.e4 (2017).
28. Wegrecki, M., Rodríguez-Galán, O., la Cruz, de, J. & Bravo, J. The structure of Erb1-Ytm1 complex reveals the functional importance of a high-affinity binding between two -propellers during the assembly of large ribosomal subunits in eukaryotes. *Nucleic Acids Research* **43**, 11017–30 (2015).
29. Kelley, L. A., Mezulis, S., Yates, C. M., Wass, M. N. & Sternberg, M. J. E. The Phyre2 web portal for protein modeling, prediction and analysis. *Nat Protoc* **10**, 845–858 (2015).
30. Emsley, P. & Cowtan, K. Coot: model-building tools for molecular graphics. *Acta Crystallogr. D Biol. Crystallogr.* **60**, 2126–2132 (2004).
31. Adams, P. D. *et al.* PHENIX: a comprehensive Python-based system for macromolecular structure solution. *Acta Crystallogr. D Biol. Crystallogr.* **66**, 213–221 (2010).
32. Pettersen, E. F. *et al.* UCSF Chimera--a visualization system for exploratory research and analysis. *J Comput Chem* **25**, 1605–1612 (2004).
33. Shi, Y. *et al.* Structural characterization by cross-linking reveals the detailed architecture of a coatomer-related heptameric module from the nuclear pore complex. *Mol. Cell Proteomics* **13**, 2927–2943 (2014).
34. Shi, Y. *et al.* A strategy for dissecting the architectures of native macromolecular assemblies. *Nat. Methods* **12**, 1135–1138 (2015).
35. Yang, B. *et al.* Identification of cross-linked peptides from complex samples. *Nat. Methods* **9**, 904–906 (2012).

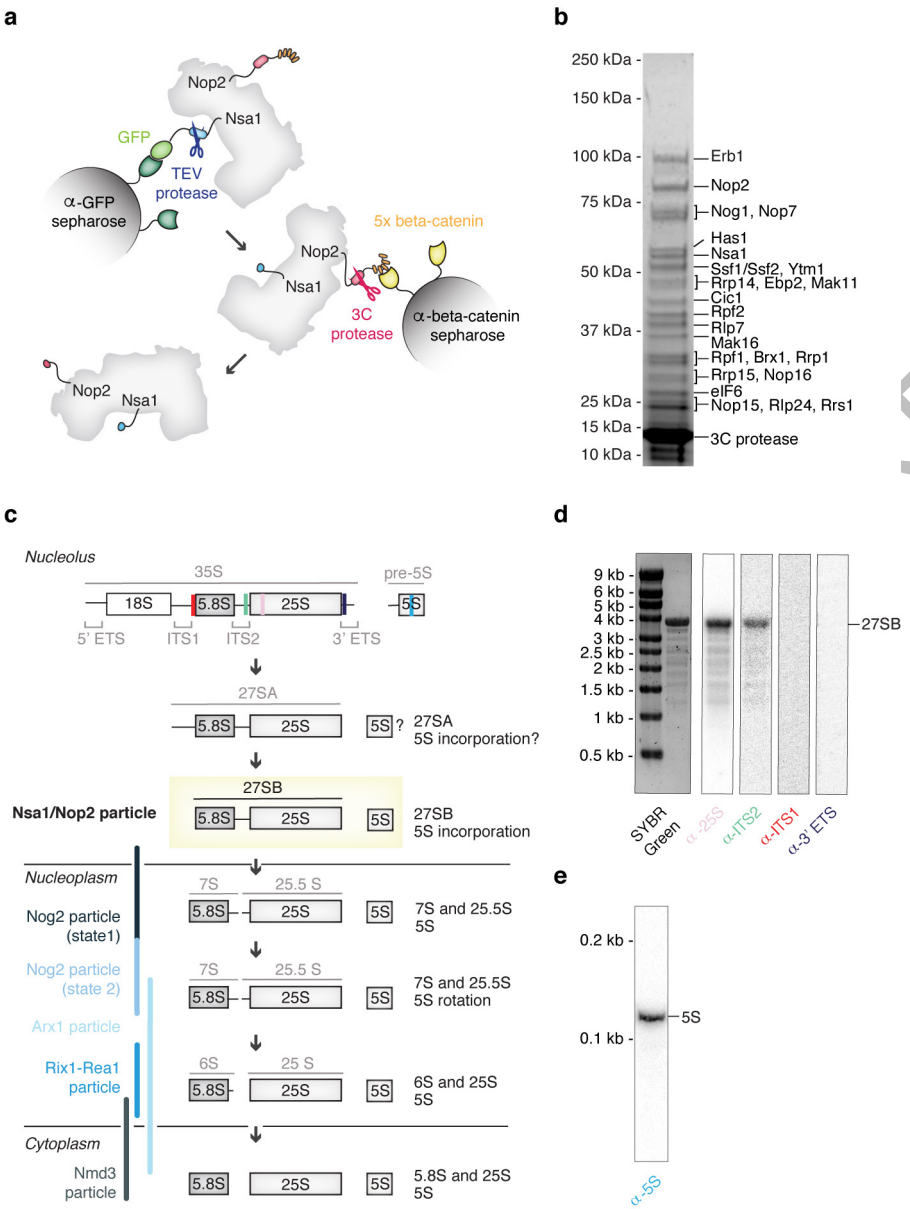

Extended Data Figure 1 | Purification of Nsa1/Nop2 tagged nucleolar pre-60S particles and analysis of RNA components. (**a**) Schematic of tandem-affinity purification for the nucleolar pre-60S particle with tagged proteins Nsa1 and Nop2. (**b**) Coomassie-blue stained SDS-PAGE of pre-60S particles purified as in (**a**). Protein labels are based on in solution mass-spectrometry analysis of purified pre-60S particles and the approximate molecular weight. (**c**) Schematic processing of the large ribosomal subunit rRNAs in yeast. The locations of the previously published pre-60S particles (the Nog2 particles[2], the Arx1 particle[19], the Rix1-Rea1 particle[3] and the Nmd3 particle[4]) are represented by blue bars. Binding sites of Northern blot probes are indicated on the 35S and pre-5S transcript. (**d**, **e**) Pre-rRNA was visualized on an agarose gel and stained using SYBR-green II. Northern blot analysis was performed for the 25S, ITS2, ITS1 and 3' ETS RNAs (**d**) and for the 5S rRNA (**e**).

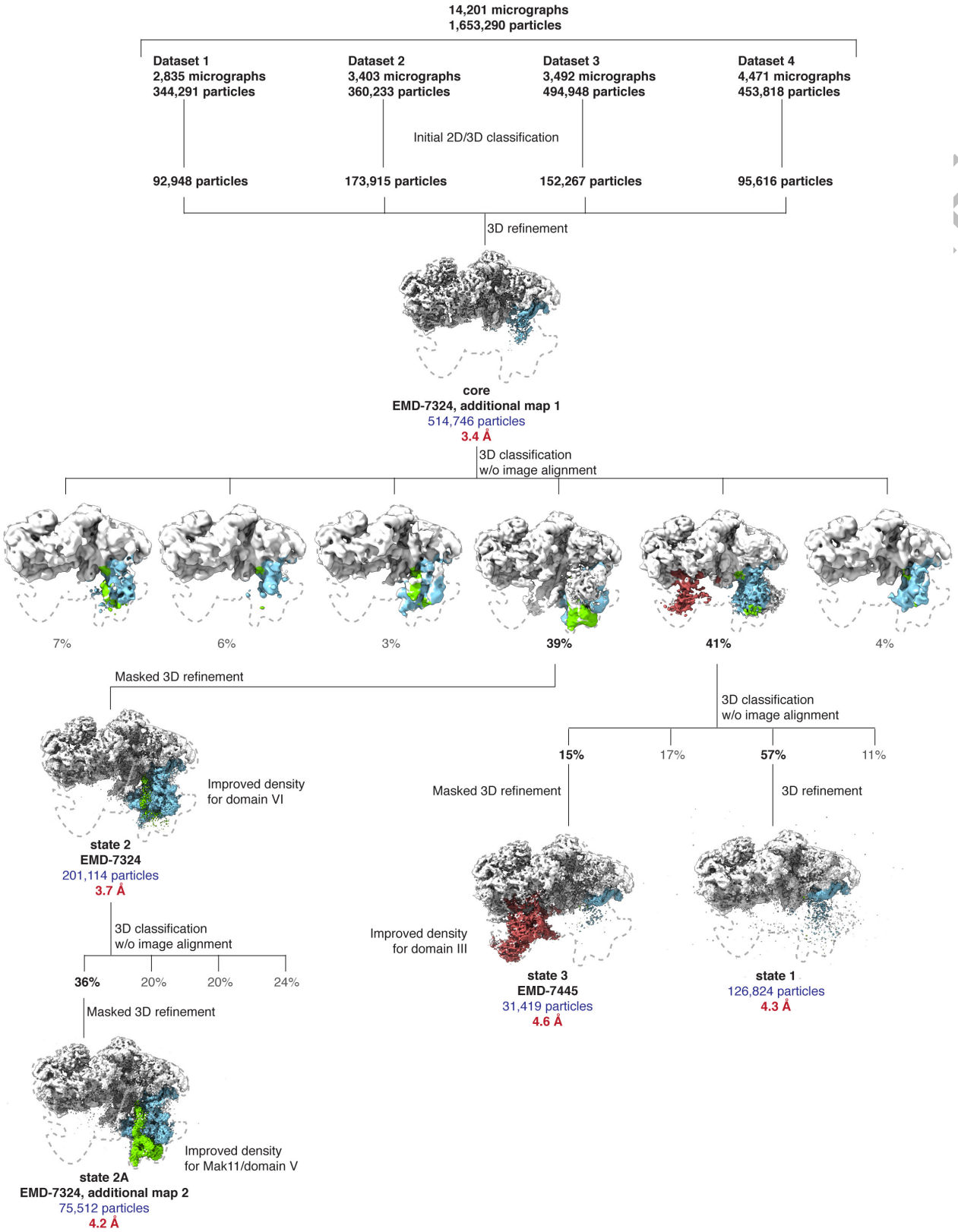

Extended Data Figure 2 | Cryo-EM data-processing workflow. 14,201 micrographs were obtained over four data collections. These micrographs were aligned using MotionCor2 (ref. 20) with dose weighting, and imported into Relion2.1 (ref. 21) for further processing. Autopicking followed by manual cleaning, 2D and 3D classification produced a total of 514,746 good particles. These particles were refined to produce the core map. Further 3D classification without and with alignment was used to obtain the state 1, state 2, state 2A and state 3 maps. Density regions corresponding to domain III (red), domain VI (blue) and Mak11 (green) are colored.

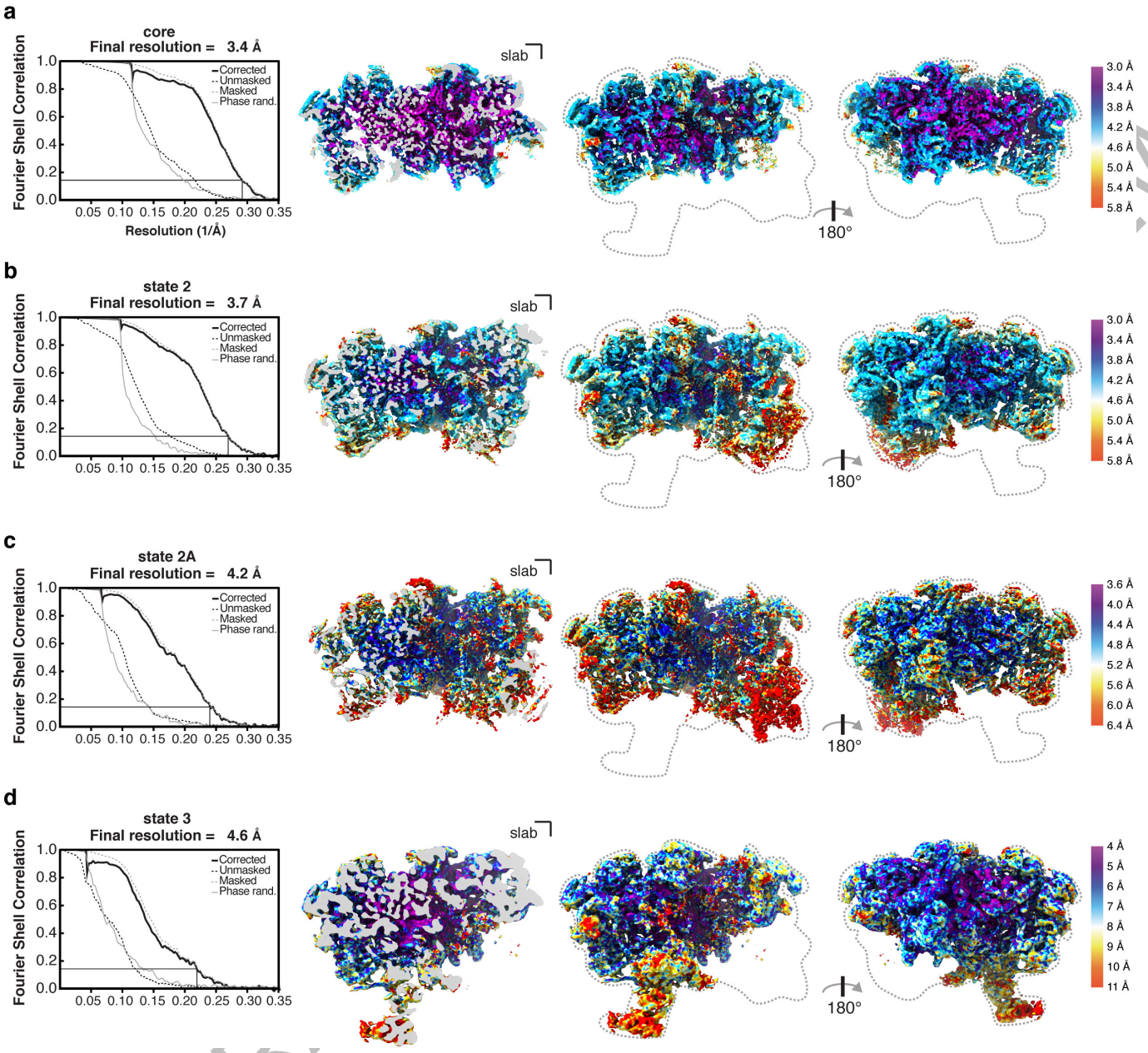

Extended Data Figure 3 | Overall and local resolution estimates for core, state 2 and state 3 cryo-EM maps. Overall and local resolution of (**a**) core map at 3.4 Å, (**b**) state 2 map at 3.7 Å, (**c**) state 2A map with additional density for Mak11 at 4.2 Å and (**d**) state 3 map at 4.6 Å. (**a**-**d**) Fourier Shell Correlation (FSC) curves for the unmasked (dashed black line), phase-randomized (solid grey line), the masked (dashed grey line) and the corrected map (solid black line). A thin black line indicates an FSC value of 0.143. A clipped view is shown next to two views of the obtained cryo-EM maps. The density volumes are colored according to local resolution using Resmap[22].

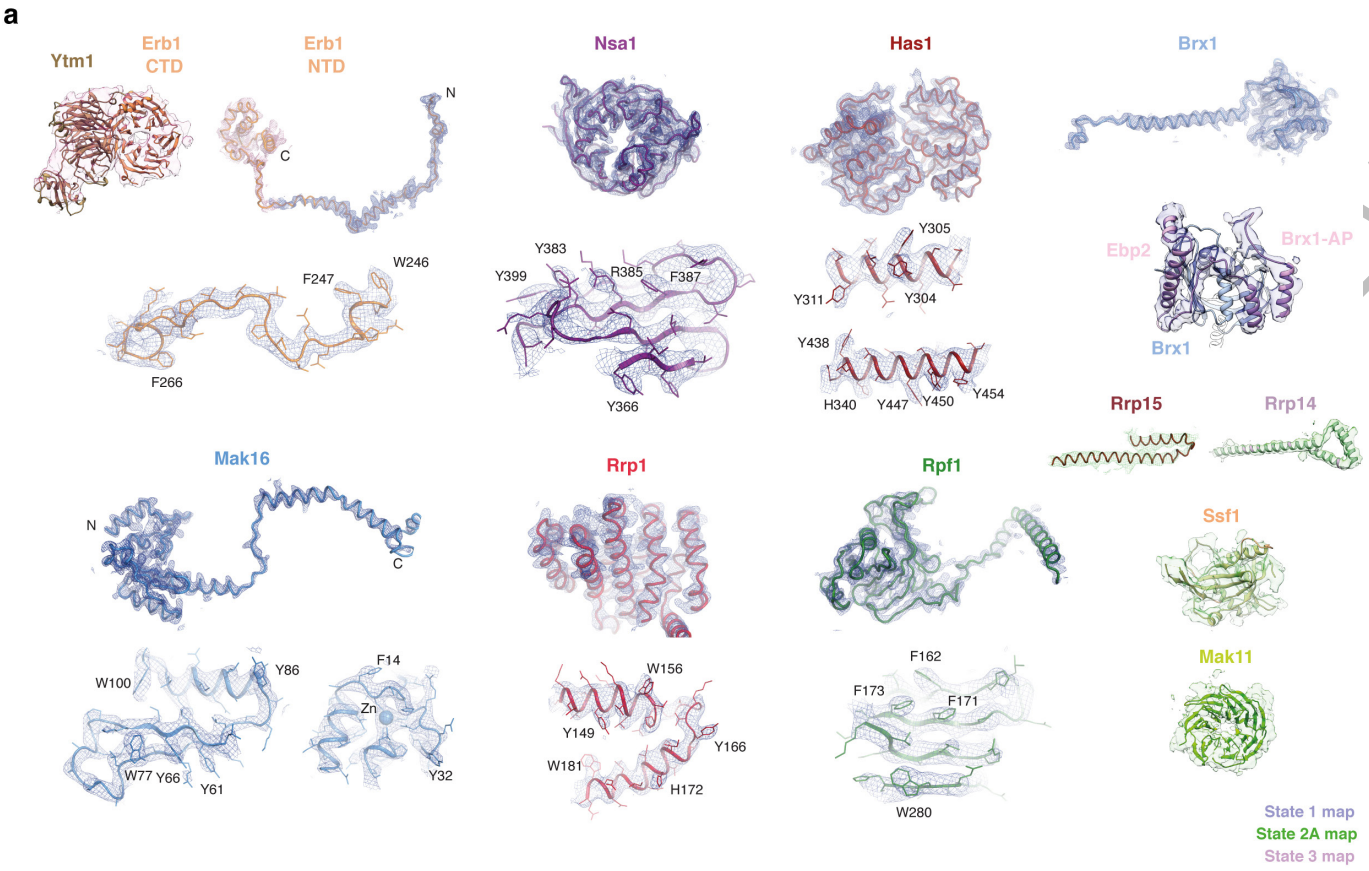

Extended Data Figure 4 | Cryo-EM density fit of selected nucleolar pre-60S ribosomal subunit proteins and RNA models. (**a**) Near atomic models of assembly factors and their cryo-EM density. (**b**) Selected regions of the 25S rRNA and 5.8S rRNA models and their cryo-EM density. Images generated in PyMOL or Chimera.

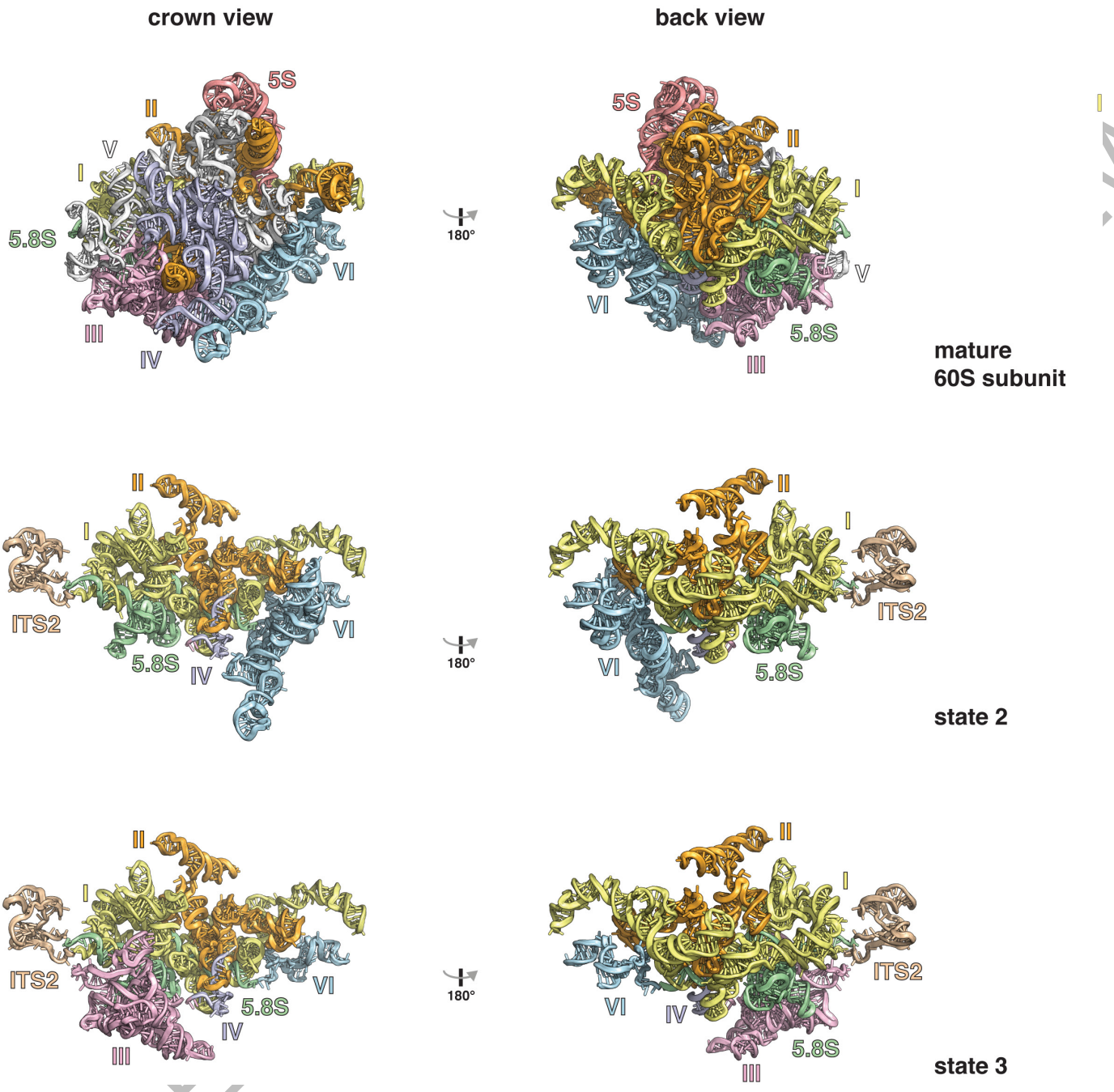

Extended Data Figure 5 | rRNA domains of state 2, state 3, and the mature 60S ribosomal subunit. The 5.8S rRNA, the 5S rRNA and the domains of the 25S rRNA are color-coded and displayed in the crown and back view for each structure.

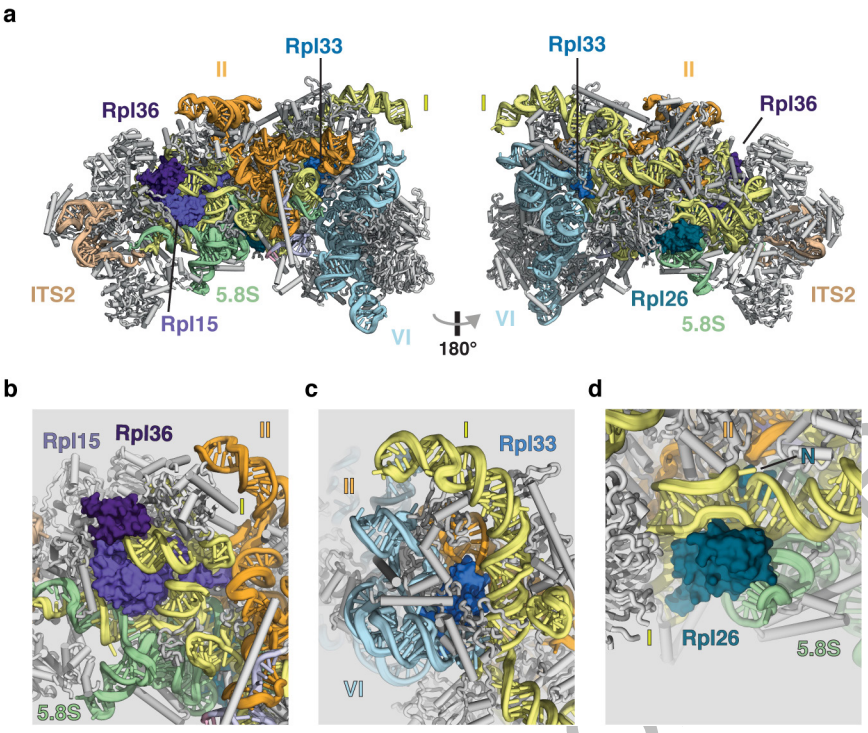

Extended Data Figure 6 | Ribosomal proteins associated with Diamond Blackfan anemia are positioned at rRNA domain junctions in the nucleolar pre-60S particle. (**a**) Two views of the nucleolar pre-60S particle state 2 model, with Diamond Blackfan anemia associated ribosomal proteins shown in surface representation. (**b**) Rpl15 is located between the 5.8S-domain I duplex and a domain I-domain II interface. (**c**) Rpl33 (Rpl35 in *H. sapiens*) binds at the domain I, II, and VI junction of the 25S rRNA. (**d**) Rpl26 associates with the domain I −5.8S rRNA interface and additionally inserts its N-terminus (N) between domain I and II.

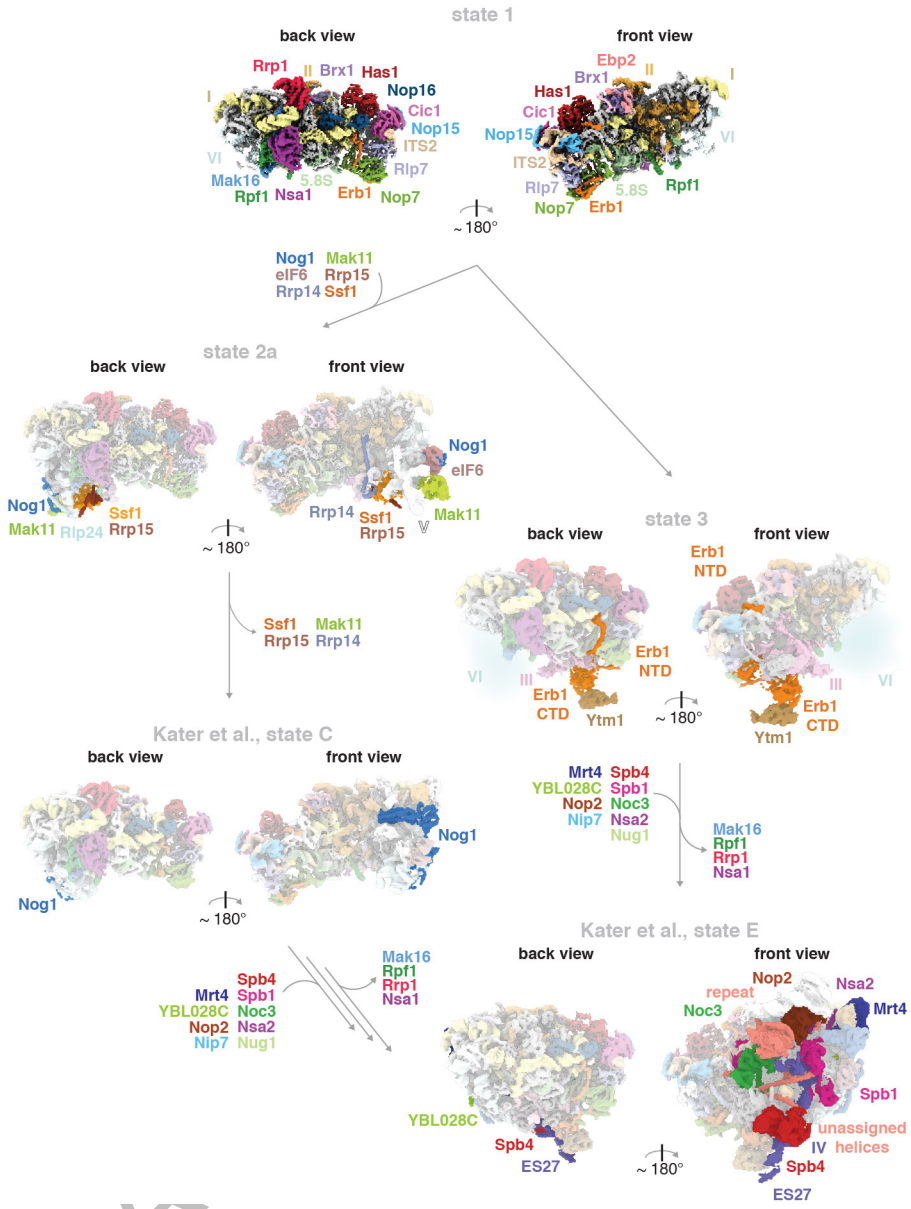

Extended Data Figure 7 | Intermediates of nucleolar pre-60S assembly. The structural data presented in this manuscript (states 1, 2, and 3) is complemented by recent data on pre-60S assembly (Kater et al., states C (EMD-3893) and E (EMD-3891)). State 1 is highly similar to Kater et al. state A (EMD-3888). States 2/2A correspond most closely to Kater et al., state B (EMD-3889), but state B lacks the Ssf1/Rrp15/Rrp14 module and Mak11. Built assembly factors that become ordered or leave in subsequent particles are indicated with arrows. Two possible pathways are shown that result in the final incorporation of the DEAD-box helicase Spb4 (previously unidentified, Kater et al.).

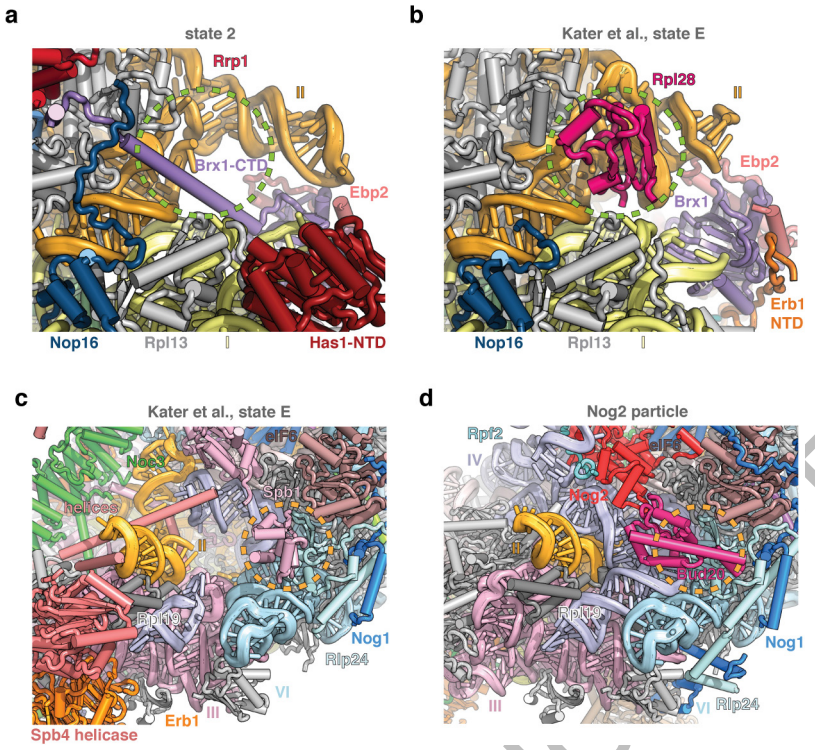

Extended Data Figure 8 | Steric hindrance during nucleolar pre-60S assembly. (**a**, **b**) Comparative views of state 2 (**a**) and Kater et al. state E (PDB 6ELZ) (**b**) highlighting that the binding of the Brx1 CTD to Rrp1 prevents premature incorporation of Rpl28. (**c**, **d**) Comparative views of state E (**c**) and the Nog2-particle (3JCT) (**d**) highlighting that the presence of Spb1 prevents the binding of Bud20.

Extended Data Table 1 | Molecular models of the nucleolar pre-60S ribosomal subunit

Subgroup	Chain ID	SegID	Molecule name	Total residues or bases	Modelled (residue range)	Initial PDB template	Present in…
RNA	1	L1	25S	3,396	atomic (1,676 bases)	3JCT	All states
	2	L2	5.8S	158	atomic (158 bases)	3JCT	All states
	6	L6	ITS2	232	atomic (87 bases)	3JCT	All states
Ribosomal proteins	C	LC	Rpl4A_uL4	362	atomic (2-56, 89-347)	3JCT	All states
	E	LE	Rpl6A_eL6	176	atomic (7-176)	3JCT	All states
	e	SE	Rpl32_eL32	130	atomic (7-36, 47-130)	3JCT	All states
	F	LF	Rpl7A_uL30	244	atomic (3-244)	3JCT	All states
	f	SF	Rpl33A_eL33	107	atomic (2-107)	3JCT	All states
	G	LG	Rpl8A_eL8	256	atomic (53-239)	3JCT	All states
	h	SH	Rpl35A_uL29	120	atomic (2-120)	3JCT	All states
	i	SI	Rpl36A_eL36	100	atomic (17-100)	3JCT	All states
	L	LL	Rpl13A_eL13	199	atomic (22-127)	3JCT	All states
	M	LM	Rpl14A_eL14	138	atomic (11-138)	3JCT	All states
	N	LN	Rpl15A_eL15	204	atomic (2-68, 96-204)	3JCT	All states
	O	LO	Rpl16A_uL13	199	atomic (3-59, 73-199)	3JCT	All states
	Q	LQ	Rpl18A_eL18	186	atomic (15-146)	4v88, chain BQ	All states
	S	LS	Rpl20A_eL20	172	atomic (2-172)	3JCT	All states
	B	LB	Rpl3_uL3	387	atomic (17-224, 270-385)	4v88, chain DB	State 2
	P	LP	Rpl17A_uL22	184	atomic (10-64, 80-126, 140-161)	3JCT	All states
	V	LV	Rpl23A_uL14	137	atomic (16-137)	3JCT	State 2
	Y	LY	Rpl26A_uL24	127	atomic (2-127)	3JCT	All states
	j	SJ	Rpl37A_eL37	88	atomic (14-85, Zn)	3JCT	All states
	Z	LZ	Rpl27A_eL27	136	side-chain trimmed (2-136)	3JCT	State 3
	k	SK	Rpl38_eL38	78	side-chain trimmed (2-78)	3JCT	State 3
	g	SG	Rpl34A_eL34	121	side-chain trimmed (2-102)	3JCT	State 3
	c	SC	Rpl30_eL30	105	side-chain trimmed (9-105)	3JCT	State 3
	X	LX	Rpl25_uL23	142	side-chain trimmed (2-142)	3JCT	State 3
Assembly factors common to Nog2 particle (3JCT)	K	LK	Cic1	376	atomic (31-51, 64-302)	3JCT	All states
	n	SN	Nop7	605	atomic (13-43, 61-267, 351-396, 404-460)	3JCT	All states
	o	SO	Nop15	220	atomic (88-220)	3JCT	All states
	t	ST	Rlp7	322	atomic (54-105, 127-322)	3JCT	All states
	t	ST	Rlp7 (NTD)	322	poly-alanine (20-53)	De novo	State 3
	u	SU	Rlp24	199	atomic (2-130, Zn)	3JCT	State 2
	y	SY	Tif6	245	atomic (1-226)	3JCT	State 2
	W	LW	Nog1	647	atomic (373-470)	3JCT	State 2
New assembly factors	A	LA	Nsa1	463	atomic (1-78, 101-416)	5SUI	All states
	p	SP	Has1	505	atomic (42-252, 264-489)	Phyre model based on 2V1X	All states
	b	SB	Brx1	291	atomic (31-122, 132-164, 174-192, 211-290), poly-alanine (123-131, 165-173)	Model based on 5WLC, chain SM	All states
	m	SM	Ebp2	427	poly-alanine (196-269)	De novo	All states
	z	SZ	Rrp1	278	atomic (1-186, 197-253)	De novo	All states
	D	LD	Mak16	306	atomic (2-191, Zn)	De novo	All states
	I	LI	Rpf1	295	atomic (8-295)	Phyre model based on 5JPQ, chain c	All states
	s	SS	Erb1-NTD	807	atomic (239-298, 372-395), poly-alanine (299-371)	De novo	All states
	s	SS	Erb1-CTD	807	side-chain trimmed crystal structure (416-426, 428-534, 571-807)	4U7A	State 3
	v	SV	Ssf1	453	atomic (23-214, 324-356)	Phyre model based on 4XV9	State 2
	q	SQ	Mak11	468	poly-alanine (WD40, 285 residues)	Phyre model based on 3DM0	States 2 and 2A
	w	SW	Rrp15	250	atomic (174-243)	De novo	State 2
	d	SD	Ytm1	460	poly-alanine (*C. thermophilum*, 465 residues)	5CXB	State 3
	7	S7	Nop16	231	atomic (1-83, 156-228)	De novo	All states
	8	S8	Rrp14	434	atomic (296-393)	De novo	State 2
	x	SX	Brx1-associated peptide	unknown	poly-alanine (162-189)	De novo	All states

Individual protein chains are listed with their initial PDB template (or built *de novo*) and the nucleolar pre-60S particle state(s) in which they are present.

nature research

Corresponding author(s): Sebastian Klinge

Life Sciences Reporting Summary

Nature Research wishes to improve the reproducibility of the work that we publish. This form is intended for publication with all accepted life science papers and provides structure for consistency and transparency in reporting. Every life science submission will use this form; some list items might not apply to an individual manuscript, but all fields must be completed for clarity.

For further information on the points included in this form, see Reporting Life Sciences Research. For further information on Nature Research policies, including our data availability policy, see Authors & Referees and the Editorial Policy Checklist.

Please do not complete any field with "not applicable" or n/a. Refer to the help text for what text to use if an item is not relevant to your study.
For final submission: please carefully check your responses for accuracy; you will not be able to make changes later.

Experimental design

1. Sample size

   Describe how sample size was determined. — No sample size calculation was performed

2. Data exclusions

   Describe any data exclusions. — No data was excluded

3. Replication

   Describe the measures taken to verify the reproducibility of the experimental findings. — Not applicable

4. Randomization

   Describe how samples/organisms/participants were allocated into experimental groups. — Not applicable

5. Blinding

   Describe whether the investigators were blinded to group allocation during data collection and/or analysis. — Not applicable

   Note: all in vivo studies must report how sample size was determined and whether blinding and randomization were used.

6. Statistical parameters

   For all figures and tables that use statistical methods, confirm that the following items are present in relevant figure legends (or in the Methods section if additional space is needed).

n/a	Confirmed
☒	☐ The exact sample size (*n*) for each experimental group/condition, given as a discrete number and unit of measurement (animals, litters, cultures, etc.)
☒	☐ A description of how samples were collected, noting whether measurements were taken from distinct samples or whether the same sample was measured repeatedly
☒	☐ A statement indicating how many times each experiment was replicated
☒	☐ The statistical test(s) used and whether they are one- or two-sided *Only common tests should be described solely by name; describe more complex techniques in the Methods section.*
☒	☐ A description of any assumptions or corrections, such as an adjustment for multiple comparisons
☒	☐ Test values indicating whether an effect is present *Provide confidence intervals or give results of significance tests (e.g. P values) as exact values whenever appropriate and with effect sizes noted.*
☒	☐ A clear description of statistics including central tendency (e.g. median, mean) and variation (e.g. standard deviation, interquartile range)
☒	☐ Clearly defined error bars in all relevant figure captions (with explicit mention of central tendency and variation)

See the web collection on statistics for biologists for further resources and guidance.

Software

Policy information about availability of computer code

7. Software

Describe the software used to analyze the data in this study.	MotionCor2, Relion, Coot, Chimera, PyMol

For manuscripts utilizing custom algorithms or software that are central to the paper but not yet described in the published literature, software must be made available to editors and reviewers upon request. We strongly encourage code deposition in a community repository (e.g. GitHub). *Nature Methods* guidance for providing algorithms and software for publication provides further information on this topic.

Materials and reagents

Policy information about availability of materials

8. Materials availability

Indicate whether there are restrictions on availability of unique materials or if these materials are only available for distribution by a third party.	No unique materials were used.

9. Antibodies

Describe the antibodies used and how they were validated for use in the system under study (i.e. assay and species).	Not applicable

10. Eukaryotic cell lines

a. State the source of each eukaryotic cell line used.	Not applicable
b. Describe the method of cell line authentication used.	Not applicable
c. Report whether the cell lines were tested for mycoplasma contamination.	Cell lines were not tested for mycoplasma contamination.
d. If any of the cell lines used are listed in the database of commonly misidentified cell lines maintained by ICLAC, provide a scientific rationale for their use.	No commonly misidentified cell lines were used.

Animals and human research participants

Policy information about studies involving animals; when reporting animal research, follow the ARRIVE guidelines

11. Description of research animals

Provide all relevant details on animals and/or animal-derived materials used in the study.	No animals were used.

Policy information about studies involving human research participants

12. Description of human research participants

Describe the covariate-relevant population characteristics of the human research participants.	The study did not involve human research participants.